

9-11-2018

Unraveling the Stereodynamics of Cold Controlled HD-H2 Collisions

James F. E. Croft

University of Nevada, Las Vegas

Naduvallath Balakrishnan

University of Nevada, Las Vegas, balakrishnan.naduvallath@unlv.edu

Meng Huang

University of New Mexico

Hua Guo

University of New Mexico

Follow this and additional works at: https://digitalscholarship.unlv.edu/chem_fac_articles

 Part of the [Chemistry Commons](#), and the [Physics Commons](#)

Repository Citation

Croft, J. F., Balakrishnan, N., Huang, M., Guo, H. (2018). Unraveling the Stereodynamics of Cold Controlled HD-H2 Collisions. *Physical Review Letters*, 121(11), 1-5.

<http://dx.doi.org/10.1103/PhysRevLett.121.113401>

This Article is protected by copyright and/or related rights. It has been brought to you by Digital Scholarship@UNLV with permission from the rights-holder(s). You are free to use this Article in any way that is permitted by the copyright and related rights legislation that applies to your use. For other uses you need to obtain permission from the rights-holder(s) directly, unless additional rights are indicated by a Creative Commons license in the record and/or on the work itself.

This Article has been accepted for inclusion in Chemistry and Biochemistry Faculty Publications by an authorized administrator of Digital Scholarship@UNLV. For more information, please contact digitalscholarship@unlv.edu.

Unraveling the Stereodynamics of Cold Controlled HD-H₂ Collisions

James F. E. Croft and Naduvalath Balakrishnan*

Department of Chemistry and Biochemistry, University of Nevada, Las Vegas, Nevada 89154, USA

Meng Huang and Hua Guo

Department of Chemistry and Chemical Biology, University of New Mexico, Albuquerque, New Mexico 87131, USA

(Received 29 June 2018; published 11 September 2018)

Measuring inelastic rates with partial-wave resolution requires temperatures close to a Kelvin or below, even for the lightest molecule. In a recent experiment, Perreault, Mukherjee, and Zare [*Nat. Chem.* **10**, 561 (2018).] studied collisional relaxation of excited HD molecules in the $v = 1$, $j = 2$ state by *para*- and *ortho*-H₂ at a temperature of about 1 K, extracting the angular distribution of scattered HD in the $v = 1$, $j = 0$ state. By state preparation of the HD molecules, control of the angular distribution of scattered HD was demonstrated. Here, we report a first-principles simulation of that experiment which enables us to attribute the main features of the observed angular distribution to a single $L = 2$ partial-wave shape resonance. Our results demonstrate important stereodynamical insights that can be gained when numerically exact quantum scattering calculations are combined with experimental results in the few-partial-wave regime.

DOI: [10.1103/PhysRevLett.121.113401](https://doi.org/10.1103/PhysRevLett.121.113401)

Introduction.—The ultimate goal of chemistry is the complete quantum state control of both reactants and products. Understanding the state-to-state stereodynamics of collision processes is a prerequisite for attaining such control [1–4]. Reducing the collision energy to a Kelvin or less simplifies collisional processes by restricting the relevant number of partial waves. Thanks to recent developments in molecule cooling and trapping [5–12] and merged beams [13–16], it is now increasingly possible to study molecular systems in this few-partial-wave regime [17–23].

The stereodynamics of many inelastic and reactive molecular encounters is strongly influenced by resonances, which occur via either tunneling through a centrifugal barrier (shape resonance) or coupling to a bound state of a closed channel (Fano-Feshbach resonance) [15,23–25]. Low-energy collisions of light molecules such as H₂ near 1 K are dominated by just a few partial waves. However, experimental studies of molecular collisions and measurements of product angular distributions in this regime have been a significant challenge, in particular, for neutral molecules such as H₂ and HD, which are not magnetically trappable and have a zero or very small dipole moment (for HD).

In a landmark experiment, Perreault, Mukherjee, and Zare reported four-vector correlations for collisions of excited HD molecules in the $v = 1$, $j = 2$ level with D₂ and H₂ at a collision energy around 1 K [1,20]. In the experiment, HD and H₂/D₂ are coexpanded in a single beam, and the HD molecules are prepared in one of two specific well-defined states using the technique of Stark-induced adiabatic Raman passage (SARP). The SARP combined with a coexpansion in a molecular beam therefore provides a powerful tool for

studying the stereodynamics of cold collisions without having to explicitly remove their kinetic energy [26].

Here, we report a first-principles simulation of the experiment of Perreault, Mukherjee, and Zare based on full-dimensional quantum scattering calculations. In doing so, we unravel the stereodynamics of the collision process and attribute the observed experimental angular distribution to a $L = 2$ shape resonance in the incoming channel. We also explain the origin of the symmetric angular distribution observed in the experiment.

Methods.—Being the simplest neutral molecule-molecule system, H₂ + H₂/HD collisions are amenable to full-dimensional quantum scattering calculations [27–30], and high-quality *ab initio* potential energy surfaces are available. In this work, we have used the full-dimensional H₂-H₂ potential of Hinde [31], which has been used extensively in recent years to study scattering of H₂ on H₂ and its isotopologs [32,33]. Its features compare well with the other available potentials for the H₂-H₂ system [34,35]. In particular, its accuracy is comparable to the four-dimensional potential of Patkowski *et al.* [35], which is considered to be the most accurate for the H₂-H₂ system (with an uncertainty of about 0.15 K or about 0.3% at the minimum of the potential well).

Scattering calculations for collisions of HD with H₂ were performed in full dimensionality using a modified version of the TwoBC code [36]. The methodology is well established and outlined in detail [30,32,37] and has been applied to other similar systems [38–41]. Here we briefly review the methodology in order to define the notation. The scattering calculations are performed within the

time-independent close-coupling formalism yielding the usual asymptotic S matrix [42]. For convenience, we label each asymptotic channel by the combined molecular state (CMS) $\alpha = v_1 j_1 v_2 j_2$, where v and j are vibrational and rotational quantum numbers, respectively, and the subscript 1 refers to HD and 2 to H_2 . The integral cross section for state-to-state rovibrationally inelastic scattering is given by

$$\sigma_{\alpha \rightarrow \alpha'} = \frac{\pi}{(2j_1 + 1)(2j_2 + 1)k_\alpha^2} \times \sum_{J, j_{12}, j'_{12}, l, l'} (2J + 1) |T_{\alpha j_{12}, \alpha' l' j'_{12}}^J|^2, \quad (1)$$

where $k^2 = 2\mu E/\hbar^2$, $T^J = 1 - S^J$, L is the orbital angular momentum, J is the total angular momentum ($\mathbf{J} = \mathbf{L} + \mathbf{j}_{12}$), and $\mathbf{j}_{12} = \mathbf{j}_1 + \mathbf{j}_2$. To compute the differential cross sections relevant to this work, we also need the scattering amplitude, which has previously been given by Schaefer and Meyer [43] in the helicity representation:

$$q_{\alpha, m_1, m_2, m_{12} \rightarrow \alpha', m'_1, m'_2, m'_{12}} = \frac{1}{2k_\alpha} \sum_J (2J + 1) \sum_{j_{12}, j'_{12}, l, l'} i^{l-l'+1} T_{\alpha j_{12}, \alpha' l' j'_{12}}^J d_{m_{12}, m'_{12}}^J(\theta) \times \langle j'_{12} m'_{12} J - m'_{12} | l' 0 \rangle \langle j_{12} m_{12} J - m_{12} | l 0 \rangle \times \langle j'_1 m'_1 j'_2 m'_2 | j'_{12} m'_{12} \rangle \langle j_1 m_1 j_2 m_2 | j_{12} m_{12} \rangle, \quad (2)$$

where $d_{m_{12}, m'_{12}}^J(\theta)$ is Wigner's reduced rotation matrix. The rovibrational state-to-state differential cross section is then given by

$$\frac{d\sigma_{\alpha \rightarrow \alpha'}}{d\Omega} = \frac{1}{(2j_1 + 1)(2j_2 + 1)} \times \sum_{m_1, m_2, m_{12}, m'_1, m'_2, m'_{12}} |q_{\alpha, m_1, m_2, m_{12} \rightarrow \alpha', m'_1, m'_2, m'_{12}}|^2. \quad (3)$$

Results.—In the recent work of Perreault, Mukherjee, and Zare, collisions of $HD(v=1, j=2)$ with $H_2(v=0, j=0, 1)$ were studied in the 0–10 K regime and the angular distribution of $HD(v=1, j=0)$ measured [1]. Figure 1 shows the corresponding theoretical integral cross section for $\alpha = 1200 \rightarrow 1000$ and $\alpha = 1201 \rightarrow 1001$. It is clearly seen that there are shape resonances for collisions with both *ortho*- H_2 and *para*- H_2 , in the vicinity of 1 K, with the dominant feature being a $L = 2$ shape resonance with *ortho*- H_2 at around 1 K.

In order to gain insight into the nature of the resonances seen in Fig. 1, we analyzed the effective potential matrix corresponding to different incoming partial waves L :

$$V_{v_1 j_1 v_2 j_2 L j_{12}, v'_1 j'_1 v'_2 j'_2 L' j'_{12}}^J(R) = \epsilon_{v_1 j_1 v_2 j_2} + \frac{L(L+1)\hbar^2}{2\mu R^2} + U_{v_1 j_1 v_2 j_2 L j_{12}, v'_1 j'_1 v'_2 j'_2 L' j'_{12}}^J(R). \quad (4)$$

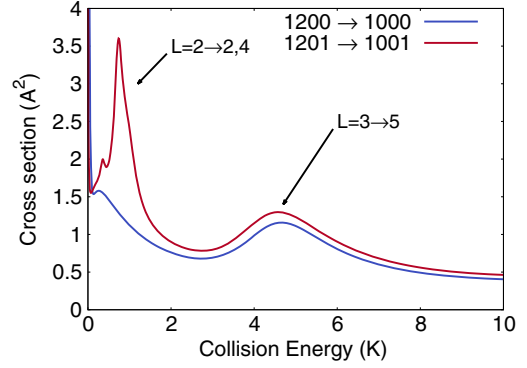


FIG. 1. Integral state-to-state cross sections for $HD(v=1, j=2) \rightarrow HD(v=1, j=0)$ in collisions with $H_2(j=0, 1)$.

The first term is the energy of the CMS obtained by adding the asymptotic rovibrational energies of HD and H_2 . The second term is the centrifugal potential for the orbital angular momentum L , and the third term is the potential energy matrix in the channel basis. At large intermolecular separations, the energies of the different channels that correspond to the same CMS converge to its asymptotic value. The effective potential matrix is diagonalized at each value of R , and the eigenvalues as a function of R correspond to a series of adiabatic potentials. Bound or quasibound states of these one-dimensional potentials correspond to HD- H_2 complexes, and the decay of the quasibound states leads to the resonances seen in Fig. 1. Figure 2 shows the potentials for the approximately good quantum number $L = 0, 1, 2, 3, 4$ for the asymptotic state 1201 along with the corresponding one-dimensional wave functions—shown at the bound or quasibound energies. It is the quasibound states at ≈ 1 K and ≈ 5 K in the $L = 2$ and 3 channels, respectively, which lead to the shape resonances seen in Fig. 1. The corresponding dominant outgoing partial waves are $L' = 2$ and 4 for $L = 2$ and $L' = 5$ for $L = 3$ as shown in Fig. 1.

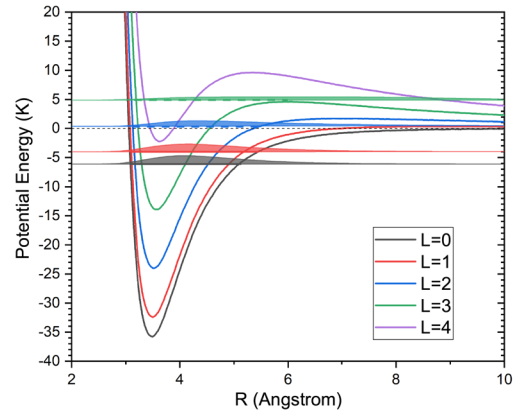


FIG. 2. One-dimensional adiabatic potentials and wave functions of the HD- H_2 system as a function of R .

The experimental setup is described in detail in a series of papers by Perreault, Mukherjee, and Zare [1,16,20]. Here we only outline the details necessary for making a comparison with our theory results. In the experiment, HD and H₂ are coexpanded in a single beam. The HD molecule is prepared in one of two specific states using the SARP technique. *H*-SARP prepares the HD($v_1 = 1, j_1 = 2$) in a state $|j_1 = 2, m_1 = 0\rangle$, where m_1 refers to the angular-momentum component along the relative velocity axis, in which case the HD bond is aligned parallel to the relative velocity. *V*-SARP prepares the HD($v_1 = 1, j_1 = 2$) in a state

$$\begin{aligned} & \sqrt{\frac{3}{8}}|j_1 = 2, m_1 = -2\rangle - \frac{1}{2}|j_1 = 2, m_1 = 0\rangle \\ & + \sqrt{\frac{3}{8}}|j_1 = 2, m_1 = 2\rangle, \end{aligned} \quad (5)$$

in which case the HD bond is aligned perpendicular to the relative velocity. The *H* and *V* in *H*-SARP and *V*-SARP refer to the horizontal and vertical orientations, respectively, of the SARP laser polarization relative to the beam velocity. The H₂, on the other hand, is not state prepared, and the ratio of *para*-H₂ to *ortho*-H₂ in the beam is taken to be 1 to 3. The experiment then measures the rate of HD($v_1 = 1, j_1 = 0$) scattered into a solid angle Ω relative to the beam velocity.

In order to compare with the experimental result, we need to account for these experimental particulars. When molecules are prepared using *H*-SARP or *V*-SARP, Eq. (3) for the differential cross section has to be modified to account for the interference between the different m 's in the initial state preparation. For *H*-SARP it becomes

$$\begin{aligned} \frac{d\sigma_{\alpha \rightarrow \alpha'}^H}{d\Omega} &= \frac{1}{(2j_2 + 1)} \\ &\times \sum_{m_2, m_{12}, m'_1, m'_2, m'_{12}} |q_{\alpha, m_1=0, m_2, m_{12} \rightarrow \alpha', m'_1, m'_2, m'_{12}}|^2, \end{aligned} \quad (6)$$

while for *V*-SARP it becomes

$$\begin{aligned} \frac{d\sigma_{\alpha \rightarrow \alpha'}^V}{d\Omega} &= \frac{1}{(2j_2 + 1)} \sum_{m_2, m_{12}, m'_1, m'_2, m'_{12}} \\ &\left| \sqrt{\frac{3}{8}} q_{\alpha, m_1=-2, m_2, m_{12} \rightarrow \alpha', m'_1, m'_2, m'_{12}} \right. \\ &\quad - \frac{1}{2} q_{\alpha, m_1=0, m_2, m_{12} \rightarrow \alpha', m'_1, m'_2, m'_{12}} \\ &\quad \left. + \sqrt{\frac{3}{8}} q_{\alpha, m_1=+2, m_2, m_{12} \rightarrow \alpha', m'_1, m'_2, m'_{12}} \right|^2. \end{aligned} \quad (7)$$

Note that Eqs. (6) and (7) are written for the general case of *H*-SARP and *V*-SARP preparation, but in the present case $m'_1 = 0$ as $j'_1 = 0$ for the scattered HD. As Fig. 1 reveals, the dominant feature seen in the experiment is expected to

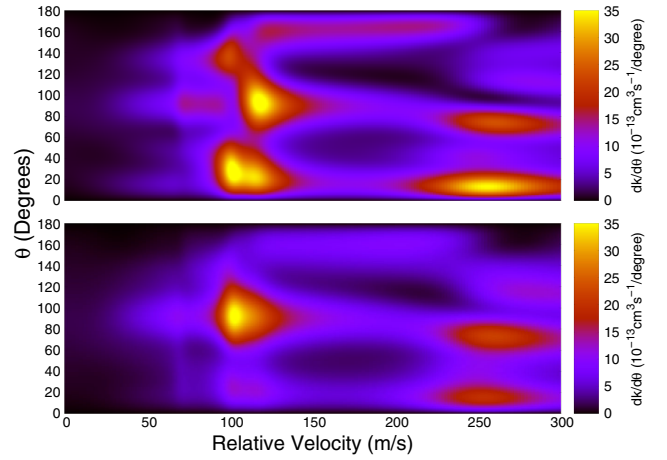


FIG. 3. The differential state-to-state rate for the transition HD($v = 1, j = 2$) \rightarrow HD($v = 1, j = 0$) in collisions with *ortho*-H₂ where the HD was prepared with *H*-SARP (upper panel) and *V*-SARP (lower panel).

be an $L = 2$ shape resonance from collisions with *ortho*-H₂, especially when the relative population of *ortho*-H₂ and *para*-H₂ in the beam is taken into account. Figure 3 shows the differential rate (defined below) as a function of the relative velocity for the state-to-state transition, HD($v = 1, j = 2$) \rightarrow HD($v = 1, j = 0$) in collisions with *ortho*-H₂ for *H*-SARP and *V*-SARP. The $L = 2$ shape resonance seen in Fig. 1 is clearly visible at around 100 ms⁻¹ (≈ 1 K). The initial alignment of the HD with respect to the beam velocity clearly makes a significant difference in the angular distribution. For *V*-SARP, where the HD bond axis is aligned perpendicular to the beam axis, the dominant scattering is at around 90°, whereas for *H*-SARP, where the HD bond axis is aligned parallel to the beam axis, there is also significant forward scattering at around 20°. The equivalent figures for collisions with *para*-H₂ are given in Supplemental Material [44].

In order to make an explicit comparison with the experimental angular distribution, we also have to average over both the relative velocity distribution and the relative populations of *ortho*-H₂ and *para*-H₂. The experimental velocity distributions for HD and H₂ are given by the Gaussian distributions $\mathcal{P}(v_{\text{HD}}) \sim \mathcal{N}(\mu_{\text{HD}} = 2814, \sigma_{\text{HD}}^2 = 71^2/2)$ and $\mathcal{P}(v_{\text{H}_2}) \sim \mathcal{N}(\mu_{\text{H}_2} = 2740, \sigma_{\text{H}_2}^2 = 105^2/2)$, respectively, where v, μ , and σ are in units of ms⁻¹ [16]. With the relative velocity defined as $v_{\text{rel}} = v_{\text{HD}} - v_{\text{H}_2}$, the relative velocity distribution is then given by convolving the two distributions yielding $\mathcal{P}(v_{\text{rel}}) \sim \mathcal{N}(\mu_{\text{rel}} = \mu_{\text{HD}} - \mu_{\text{H}_2}, \sigma_{\text{rel}}^2 = \sigma_{\text{HD}}^2 + \sigma_{\text{H}_2}^2)$. In the experiment, the scattering angle θ_{exp} is defined relative to the beam velocity; therefore, for positive relative velocities (HD catching up with H₂) $\theta_{\text{exp}} = \theta$, whereas for negative relative velocities (HD being caught up by H₂) $\theta_{\text{exp}} = \pi - \theta$. The velocity-averaged differential rate, for *ortho*- or *para*-H₂, is therefore given by

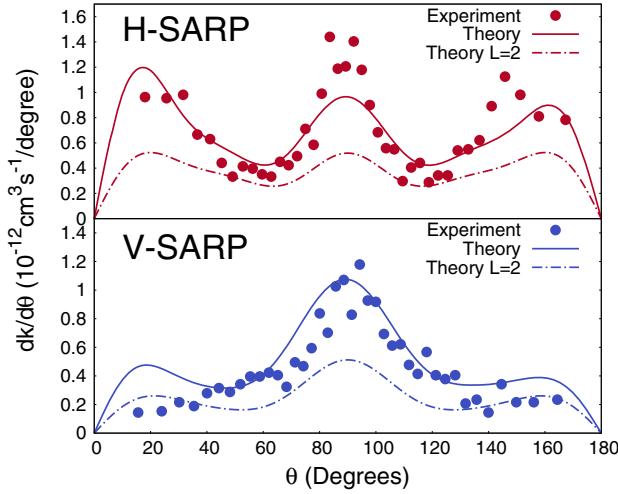


FIG. 4. The velocity-averaged differential state-to-state rate for $\text{HD}(v=1, j=2) \rightarrow \text{HD}(v=1, j=0)$ in collisions with *para*- H_2 and *ortho*- H_2 for HD prepared using *H*-SARP and *V*-SARP. The solid dots are the corresponding experiment results of Perreault, Mukherjee, and Zare [1].

$$\begin{aligned} \frac{dk(\theta_{\text{exp}})}{d\theta_{\text{exp}}} = & \int_{-\infty}^0 |v_{\text{rel}}| \frac{d\sigma(\pi - \theta)}{d\theta} P(v_{\text{rel}}) dv_{\text{rel}} \\ & + \int_0^{\infty} |v_{\text{rel}}| \frac{d\sigma(\theta)}{d\theta} P(v_{\text{rel}}) dv_{\text{rel}}; \end{aligned} \quad (8)$$

by weighting them with the experimental population of *para*- and *ortho*- H_2 (25% and 75%, respectively), a direct comparison can be made with the experiment.

Figure 4 compares our theory results with the experimental data presented in Perreault, Mukherjee, and Zare [1]. The experimental results for both *H*-SARP and *V*-SARP have been scaled by the same factor (0.009). It is seen that we find very good agreement with the experimental results, capturing the main features as well as getting the relative magnitude of *H*-SARP and *V*-SARP correct. We note that this means we also get agreement with the higher integral rate reported for *H*-SARP compared to *V*-SARP. Comparing Fig. 4 with Fig. 3, we are able to attribute the observed features to a specific resonance. This is especially clear in the case of *V*-SARP where the strong central feature is clearly due to the $L=2$ shape resonance found at 100 ms^{-1} . The $L=2$ contribution for collisions with *ortho*- H_2 is explicitly shown in Fig. 4 as dashed lines, which can be seen to make up over half of the observed rate as well as giving the overall form to the angular distribution. In the case of *H*-SARP, however, there is a backwards scattering feature (at around 160°) seen in the experiment which is not present in the theoretical differential cross sections shown in Fig. 3. This apparent backwards scattering is, in fact, the result of the velocity averaging of Eq. (8) and is actually forward scattering of HD from collisions with negative relative velocities. More generally, the

approximate symmetry of the measured angular distribution seen here is a direct consequence of the approximate symmetry of the relative velocity distribution of this kind of experimental setup, which leads to nearly equal contributions from positive and negative relative velocities in Eq. (8). The separate contributions to the angular distribution from positive and negative velocities are given in Supplemental Material [44]. We are therefore able to unambiguously attribute the observed feature to an $L=2$ shape resonance for collisions of $\text{HD}(v=1, j=2)$ with $\text{H}_2(j=1)$. We note that there is also a large $L=2$ shape resonance for collisions of $\text{HD}(v=0, j=2)$ with $\text{H}_2(j=0)$ between 0.1 and 1 K which disappears for $\text{HD}(v=1)$. If this resonance is also present for $\text{HD}(v=1)$, say, if the potential well were actually slightly deeper, it would not change this conclusion, as it would affect only the overall magnitude of the cross section but not its form [we have checked this explicitly by computing the $\text{HD}(v=0, j=2) \rightarrow \text{HD}(v=0, j=0)$ cross sections].

Conclusions.—We have performed numerically exact quantum scattering calculations for low-energy collisions of quantum-state-prepared HD with H_2 , finding good agreement with the experiment for the angular distribution of scattered HD. Our computations provide a complete numerical simulation of the experiment with full quantum-state resolution, including the orientation of the HD molecule relative to the molecular beam axis. We were able to unravel the stereodynamics of the collision process and attribute the observed angular distribution to a single $L=2$ shape resonance in the incoming channel. This demonstrates the enormous potential of low-energy beam experiments for controlled studies of inelastic collisions at the single partial-wave level and the unique insights that can be gained in the collision dynamics when combined with numerically exact scattering calculations. The stereodynamic control is achieved in the experiment by the ability to choose a single or a coherent superposition of quantum states with m -state resolution. The overall good agreement between the theory and experiment for this benchmark system also provides an independent confirmation of the accuracy of the H_2 - H_2 interaction potential for collisional studies near 1 K, a regime also of significant interest in astrophysics. Whether the small remaining discrepancies in the angular distributions can be addressed with further refinement of the H_2 - H_2 interaction potential is an issue worth exploring.

We acknowledge support from the U.S. Army Research Office, MURI Grant No. W911NF-12-1-0476 (N.B.), the U.S. National Science Foundation, Grant No. PHY-1505557 (N.B.), and Department of Energy, Grant No. DE-SC0015997 (H.G.). We thank Dick Zare, Nandini Mukherjee, and William Perreault for many stimulating discussions and for sharing their experimental data.

*naduvala@unlv.nevada.edu

- [1] W. E. Perreault, N. Mukherjee, and R. N. Zare, *Nat. Chem.* **10**, 561 (2018).
- [2] R. B. Bernstein, D. R. Herschbach, and R. D. Levine, *J. Phys. Chem.* **91**, 5365 (1987).
- [3] R. N. Zare, *Science* **279**, 1875 (1998).
- [4] J. Aldegunde, M. P. de Miranda, J. M. Haigh, B. K. Kendrick, V. Sáez-Rábanos, and F. J. Aoiz, *J. Phys. Chem. A* **109**, 6200 (2005).
- [5] R. Wynar, R. S. Freeland, D. J. Han, C. Ryu, and D. J. Heinzen, *Science* **287**, 1016 (2000).
- [6] C. A. Regal, C. Ticknor, J. L. Bohn, and D. S. Jin, *Nature (London)* **424**, 47 (2003).
- [7] B. C. Sawyer, B. L. Lev, E. R. Hudson, B. K. Stuhl, M. Lara, J. L. Bohn, and J. Ye, *Phys. Rev. Lett.* **98**, 253002 (2007).
- [8] E. S. Shuman, J. F. Barry, and D. DeMille, *Nature (London)* **467**, 820 (2010).
- [9] M. T. Hummon, M. Yeo, B. K. Stuhl, A. L. Collopy, Y. Xia, and J. Ye, *Phys. Rev. Lett.* **110**, 143001 (2013).
- [10] N. Akerman, M. Karpov, Y. Segev, N. Bibelnik, J. Narevicius, and E. Narevicius, *Phys. Rev. Lett.* **119**, 073204 (2017).
- [11] L. Anderegg, B. L. Augenbraun, E. Chae, B. Hemmerling, N. R. Hutzler, A. Ravi, A. Collopy, J. Ye, W. Ketterle, and J. M. Doyle, *Phys. Rev. Lett.* **119**, 103201 (2017).
- [12] S. Truppe, H. Williams, M. Hambach, L. Caldwell, N. Fitch, E. Hinds, B. Sauer, and M. Tarbutt, *Nat. Phys.* **13**, 1173 (2017).
- [13] A. B. Henson, S. Gersten, Y. Shagam, J. Narevicius, and E. Narevicius, *Science* **338**, 234 (2012).
- [14] J. Jankunas, B. Bertsche, K. Jachymski, M. Hapka, and A. Osterwalder, *J. Chem. Phys.* **140**, 244302 (2014).
- [15] A. Klein *et al.*, *Nat. Phys.* **13**, 35 (2017).
- [16] W. E. Perreault, N. Mukherjee, and R. N. Zare, *Chem. Phys.*, DOI: 10.1016/j.chemphys.2018.02.017 (2018).
- [17] S. Ospelkaus, K.-K. Ni, D. Wang, M. H. G. de Miranda, B. Neyenhuis, G. Quémener, P. S. Julienne, J. L. Bohn, D. S. Jin, and J. Ye, *Science* **327**, 853 (2010).
- [18] S. Knoop, F. Ferlaino, M. Berninger, M. Mark, H.-C. Nägerl, R. Grimm, J. P. D’Incao, and B. D. Esry, *Phys. Rev. Lett.* **104**, 053201 (2010).
- [19] J. Rui, H. Yang, L. Liu, D.-C. Zhang, Y.-X. Liu, J. Nan, Y.-A. Chen, B. Zhao, and J.-W. Pan, *Nat. Phys.* **13**, 699 (2017).
- [20] W. E. Perreault, N. Mukherjee, and R. N. Zare, *Science* **358**, 356 (2017).
- [21] J. Wolf, M. Deiß, A. Krütkow, E. Tiemann, B. P. Ruzic, Y. Wang, J. P. D’Incao, P. S. Julienne, and J. H. Denschlag, *Science* **358**, 921 (2017).
- [22] A. P. P. van der Poel, P. C. Zieger, S. Y. T. van de Meerakker, J. Loreau, A. van der Avoird, and H. L. Bethlem, *Phys. Rev. Lett.* **120**, 033402 (2018).
- [23] C. Amarasinghe and A. G. Suits, *J. Phys. Chem. Lett.* **8**, 5153 (2017).
- [24] D. W. Chandler, *J. Chem. Phys.* **132**, 110901 (2010).
- [25] A. Bergeat, J. Onvlee, C. Naulin, A. van der Avoird, and M. Costes, *Nat. Chem.* **7**, 349 (2015).
- [26] N. Mukherjee, W. E. Perreault, and R. N. Zare, in *Frontiers and Advances in Molecular Spectroscopy*, edited by J. Laane (Elsevier, Amsterdam, 2018).
- [27] S. Y. Lin and H. Guo, *J. Chem. Phys.* **117**, 5183 (2002).
- [28] S. K. Pogrebnya and D. C. Clary, *Chem. Phys. Lett.* **363**, 523 (2002).
- [29] F. Gatti, F. Otto, S. Sukiasyan, and H.-D. Meyer, *J. Chem. Phys.* **123**, 174311 (2005).
- [30] G. Quémener, N. Balakrishnan, and R. V. Krems, *Phys. Rev. A* **77**, 030704 (2008).
- [31] R. J. Hinde, *J. Chem. Phys.* **128**, 154308 (2008).
- [32] S. F. dos Santos, N. Balakrishnan, S. Lepp, G. Quémener, R. C. Forrey, R. J. Hinde, and P. C. Stancil, *J. Chem. Phys.* **134**, 214303 (2011).
- [33] N. Balakrishnan, G. Quémener, R. C. Forrey, R. J. Hinde, and P. C. Stancil, *J. Chem. Phys.* **134**, 014301 (2011).
- [34] A. I. Boothroyd, J. E. Dove, W. J. Keogh, P. G. Martin, and M. R. Peterson, *J. Chem. Phys.* **95**, 4331 (1991).
- [35] K. Patkowski, W. Cencek, P. Jankowski, K. Szalewicz, J. B. Mehl, G. Garberoglio, and A. H. Harvey, *J. Chem. Phys.* **129**, 094304 (2008).
- [36] R. Krems, *TwoBC—Quantum Scattering Program* (University of British Columbia, Vancouver, Canada, 2006).
- [37] G. Quémener and N. Balakrishnan, *J. Chem. Phys.* **130**, 114303 (2009).
- [38] B. Yang, P. Zhang, X. Wang, P. Stancil, J. Bowman, N. Balakrishnan, and R. Forrey, *Nat. Commun.* **6**, 6629 (2015).
- [39] B. Yang, P. Zhang, C. Qu, X. H. Wang, P. C. Stancil, J. M. Bowman, N. Balakrishnan, B. M. McLaughlin, and R. C. Forrey, *J. Phys. Chem. A* **122**, 1511 (2018).
- [40] B. Yang, X. H. Wang, P. C. Stancil, J. M. Bowman, N. Balakrishnan, and R. C. Forrey, *J. Chem. Phys.* **145**, 224307 (2016).
- [41] S. F. dos Santos, N. Balakrishnan, R. C. Forrey, and P. C. Stancil, *J. Chem. Phys.* **138**, 104302 (2013).
- [42] A. M. Arthurs and A. Dalgarno, *Proc. R. Soc. A* **256**, 540 (1960).
- [43] J. Schaefer and W. Meyer, *J. Chem. Phys.* **70**, 344 (1979).
- [44] See Supplemental Material at <http://link.aps.org/supplemental/10.1103/PhysRevLett.121.113401> for *H*-SARP and *V*-SARP differential cross sections for para- H_2 and the separate contributions to the velocity averaged result from ortho- and para- H_2 for positive and negative velocities.